



# An investigation into microstructure and mechanical properties of cold sprayed 7075 Al deposition

M.R. Rokni\*, C.A. Widener, G.A. Crawford, M.K. West

*Department of Materials & Metallurgical Engineering, Advanced Materials Processing Center, South Dakota School of Mines & Technology (SDSM&T), SD, USA*



## ARTICLE INFO

### Article history:

Received 1 October 2014

Received in revised form

16 November 2014

Accepted 18 November 2014

Available online 5 December 2014

### Keywords:

Aluminum

Cold spraying

Microstructure

Nanoindentation

Electron microscopy

## ABSTRACT

Cold spray deposition is well known to produce a highly deformed microstructure with large strain gradients across the individual particles composing the deposited layer. This study investigates the relationship between the as-deposited cold spray microstructure and the resulting local and coating-scale mechanical properties of 7075 aluminum powder deposited onto wrought 7075 aluminum substrates via high pressure cold spray. Local mechanical property variations were probed using nanoindentation and correlated with microstructural characterization conducted via various microscopy techniques. 7075 Aluminum powder particles experienced high deformation rates during impact, resulting in local microstructural variations, specifically grain size and dislocation densities, between particle interfaces and their interiors. Consequently, an average 0.5 GPa increase in nanohardness was observed in particle interface regions. This increase in hardness was concluded to be primarily the result of grain refinement promoted by local dynamic recrystallization, rather than from an increase in local dislocation density causing strain hardening behavior. Examination of the coating revealed a decrease in hardness and an increase in local grain size with increasing distance from the substrate. The effects of these microstructural variations on the quality of the deposition were also evaluated by tensile pull-off and three lug shear testing.

© 2014 Elsevier B.V. All rights reserved.

## 1. Introduction

Cold spray systems may be classified as high-pressure cold spray (HPCS) and low-pressure cold spray (LPCS), based on the level of the working gas pressure. Recently, HPCS systems have become popular because they overcome several shortcomings of more conventional LPCS systems. One of the most important improvements is the reduction in void and porosity levels in the deposited layer, owing to the much higher particle velocities and temperatures achieved with HPCS systems. As a result, highly consolidated layers with improved mechanical properties may be produced [1–5]. In order to better understand the reasons for the associated improvements in properties, however, there is a need to understand the relationship between the local microstructure and the mechanical properties in the cold spray deposition.

While particles indeed experience very large strains, the deformations are non-homogenous. This results in the presence of UFG or pancaked structures at particle–particle interfaces and larger grain size (micron size) and heavy dislocation density in particle interiors [6]. The observation of nonuniform deformation

within the cold spray deposition has also been reported for single splats [7] and for multi-layered coatings [8–11] and has been linked to inhomogeneous local mechanical properties in the cold spray layer. Finite-element analysis (FEA) employed by various research groups [12–14] has also predicted the presence of inhomogeneous deformation during cold spray processing. Results show particle interfaces experience very large strains ( $\epsilon \sim 10$ ), whereas particle interiors experience significantly less ( $\epsilon < 1$ ).

To evaluate the effects of the deformation inhomogeneity in cold spray processed (CSP) deposits, on final mechanical properties, a large number of studies have used microhardness or tensile testing [15–18]. While these techniques are indeed common and many times provide useful information, the planar geometry of the coatings make it difficult to obtain representative bulk mechanical property information. Owing to a small load ( $\sim 1$  mN) and displacement ( $\sim 1$  nm) resolution, nanoindentation testing is well suited to characterize the mechanical properties of these coatings [7,11,19–35]. This technique has been used to measure the elastic modulus of cold spray coatings [21], as well as the nanohardness of as-received metal powders [19,20] and cold spray deposited pure metals [11,22–26], metal alloys [27–31], and composite materials [32–34]. Furthermore, several nanoindentation studies have investigated the variation in local mechanical properties of cold spray coatings. These studies, however, have been restricted to pure metals (i.e. Ti [7], Al [11], Ni [26], and Cu

\* Corresponding author. Tel.: +1 605 8776902; fax: +1 605 3945246.

E-mail addresses: [reza.rokni@mines.sdsmt.edu](mailto:reza.rokni@mines.sdsmt.edu), [mreza.rokni@gmail.com](mailto:mreza.rokni@gmail.com) (M.R. Rokni), [grant.crawford@sdsmt.edu](mailto:grant.crawford@sdsmt.edu) (G.A. Crawford).

[26]) with little reported on mechanical property variation in alloy coatings (5083 Al alloy [27]). Thus, limited attention has been dedicated to studying the local mechanical property variation of critical engineering alloys (e.g. 7xxx Al alloys). Furthermore, this study advances the understanding of microstructural evolution in CSP deposits, specifically grain refinement mechanisms in cold spray deposits of 7075 Al.

The 7000 series Al alloys are a class of high strength, precipitation hardenable alloys which contain zinc as the primary alloying component. Among these alloys, the 7075 Al alloy, which is the

most popular, and has many applications in the aerospace and automotive industries due to a high strength-to-weight ratio and good corrosion resistance [35–37]. This study investigates the microstructure and mechanical property relationships before and after cold spray processing of gas atomized 7075 Al powder onto a 7075 Al substrate. Local mechanical property variation was probed using nanoindentation and correlated with microstructural analysis conducted via electron backscatter diffraction and transmission electron microscopy. The effect of microstructural variation on deposition quality was also evaluated by microhardness testing and adhesion testing (i.e. tensile pull-off and three lug shear testing).

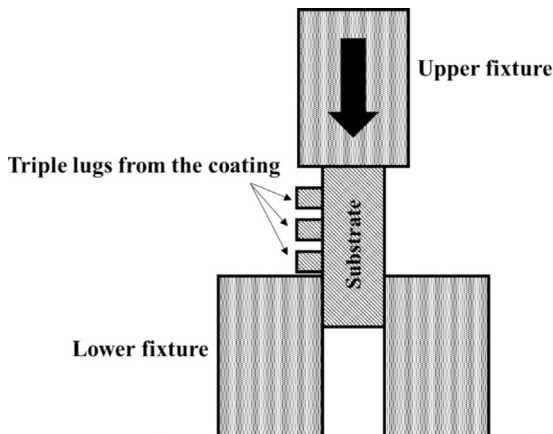


**Fig. 1.** Schematic of the shear test fixture (after [4]).

## 2. Experimental procedure

### 2.1. Cold spray processing

7075 Al (Al-6.09 Zn-2.68Mg-1.28Cu-0.18Fe-0.13 wt% Si) coatings were produced using commercially available gas-atomized 7075 Al powder (Valimet, Stockton, CA, USA),  $18.6 \pm 8.2 \mu\text{m}$  in size, deposited on a wrought 7075-T73 aluminum alloy substrate. Feedstock powder size was measured using a laser diffraction particle size analyzer (Microtrac S3000, Microtrac Software Co., Wyomissing, PA). Helium was used as the process gas to achieve high impact velocities between incident particles. The deposits were made using a VRC Gen III high-pressure cold spray system (VRC Metal Systems, Rapid City, SD, USA) and the pressure and temperature of helium were maintained at 2.8 MPa and 400 °C at the heater exit, respectively. Deposition took place using a nozzle stand-off distance of 25 mm, 90° deposition angle, medium

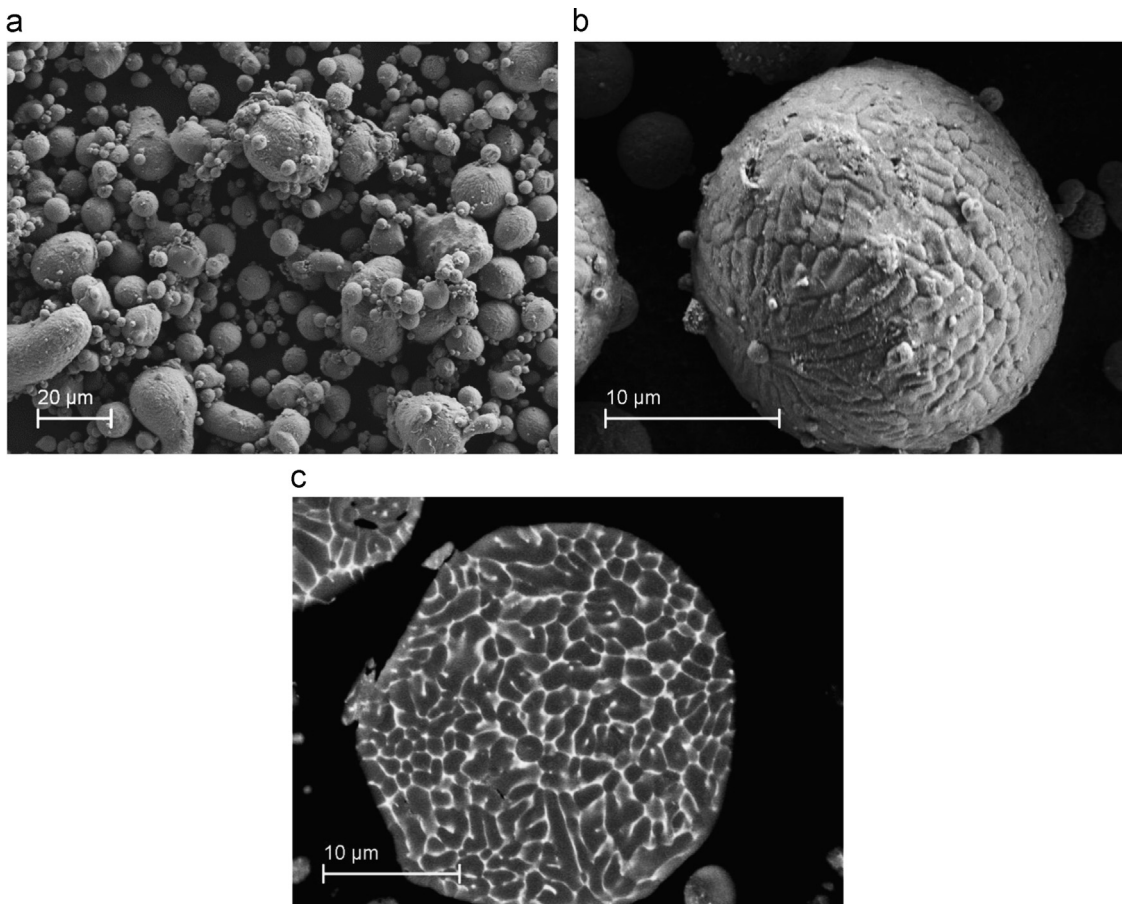


**Fig. 2.** SEM micrographs of the as-received 7075 Al powder showing; (a) powder morphology, (b) surface grain structure, and (c) BSE image showing internal grain structure and solute segregation at grain boundaries of powder particles.

powder feed rate ( $12 \text{ g min}^{-1}$ ), and a high nozzle traveling speed ( $600 \text{ mm s}^{-1}$ ). Finally, a total deposition thickness of  $\sim 8.5 \text{ mm}$  was achieved in this study.

## 2.2. Microstructural evaluation

The microstructure of the as-received powder and cold spray processed (CSP) 7075 Al layer were evaluated by optical microscopy (OM), scanning electron microscopy (SEM), electron back-scattered diffraction (EBSD) and transmission electron microscopy (TEM). EBSD samples were sectioned from the CSP layer and prepared by standard metallographic techniques. Final polish was conducted using a colloidal silica ( $\sim 0.05 \mu\text{m}$  diameter) suspension and vibratory polishing. For backscattered electron (BSE) observations of the powder particles, the powders were mounted in epoxy resin prior to standard metallographic preparation (i.e. grinding and polishing). TEM micrographs were obtained by using a JEM-2100 LaB<sub>6</sub> TEM at an accelerating voltage of 200 kV. Thin discs, 3 mm in diameter, were excised from the deposition, and then polished, dimpled, and ion milled for 4 h.

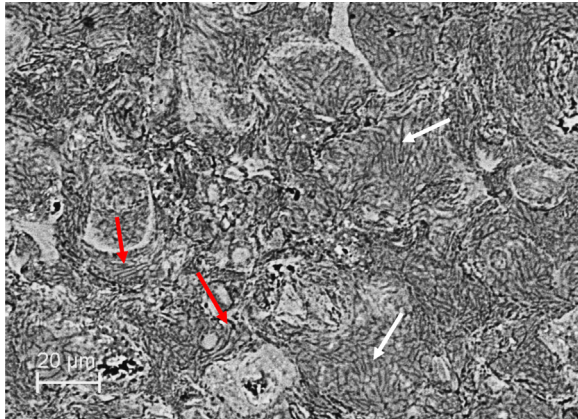


**Fig. 3.** Optical micrograph from the cross-section (perpendicular to deposition) of the CSP 7075 Al deposit. Red arrows show severely deformed structures, whereas white arrows show similar microstructure to the as-received powder.

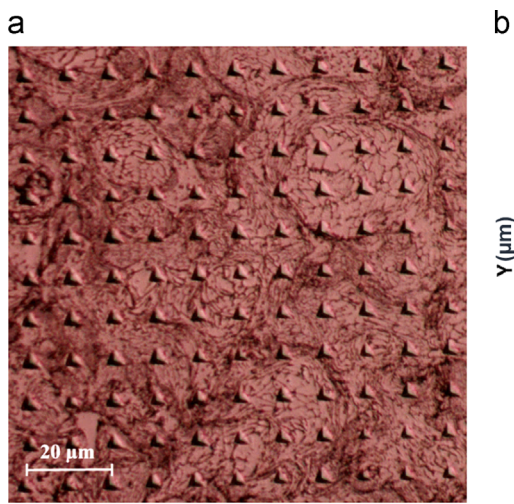


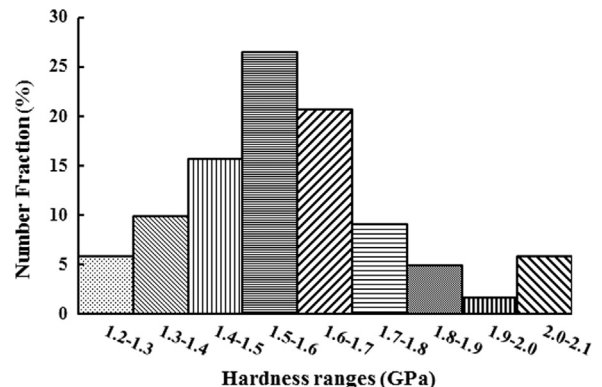
**Fig. 4.** (a) Optical micrograph showing a square array of nanoindentations on the CSP 7075 Al deposit, and (b) a contour plot of nanohardness versus position within the CSP layer.

## 2.3. Mechanical properties

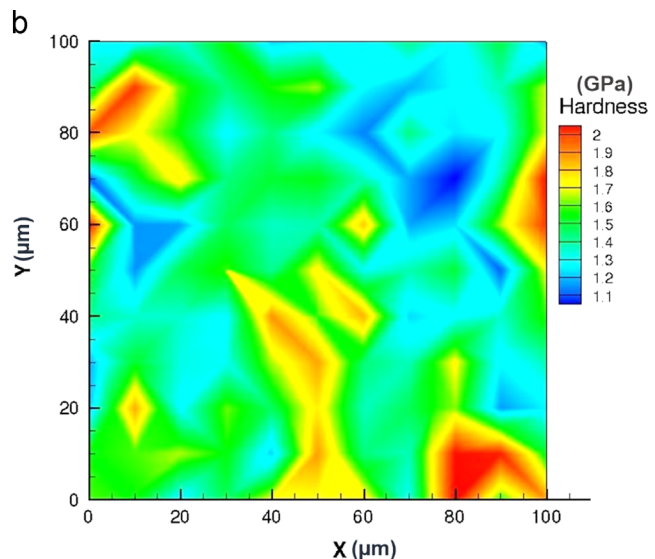
### 2.3.1. Adhesion and shear strength

The adhesion strength of the cold spray coating to the underlying substrate was evaluated using a standard tensile pull-off method (ASTM C633). Per the specification, the coating was ground to an 8 mm thickness to create a uniform surface. The coated surface was then bonded to a bare slug using a high-performance epoxy adhesive (FM1000, Cytec Industries, Woodland Park, NJ). The coupon dimensions used for adhesion testing had a diameter of 25 mm. Adhesion testing was carried out using a servo-hydraulic uniaxial testing system (MTS, Systems Corporation, Eden Prairie, MN) in displacement control with a crosshead speed of 10 mm/min. Maximum load at failure was recorded and the maximum tensile stress reported as the adhesion strength of the coating. Failed samples were visually inspected to determine the mode of failure. The primary failure modes of interest in this system include; (1) adhesive failure at coating/substrate interface, (2) cohesive failure of the coating, and (3) cohesive failure of the glue. Three samples were tested and the average adhesion strength was reported.

To study the adhesive shear behavior of the CSP deposition, a three lug shear test (MIL-J-24445A [38]) was performed. The specimens were tested in shear in a universal tensile testing



**Fig. 5.** Histogram showing the local nanohardness distribution for nanoindentations shown in Fig. 4(a).



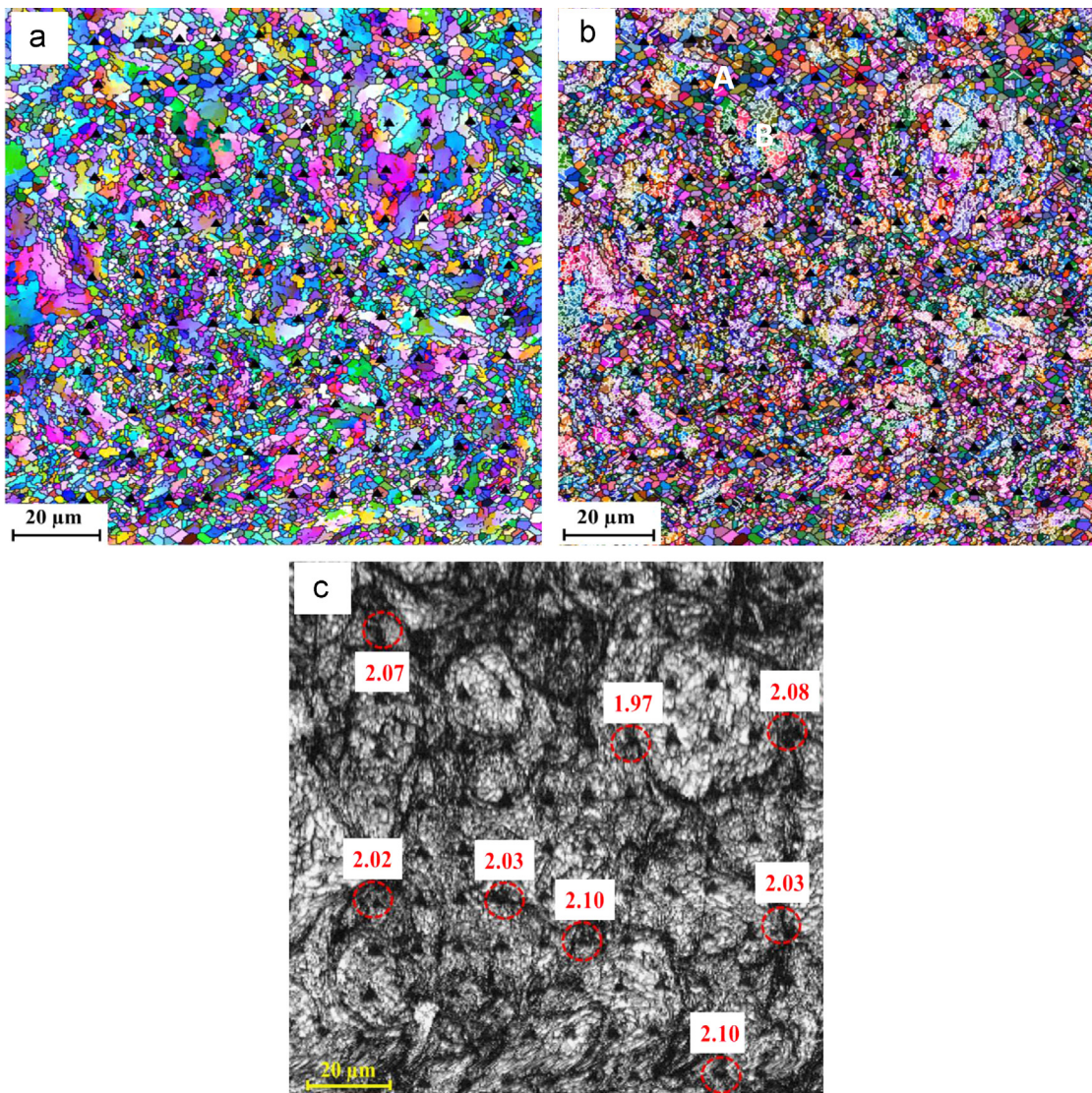


**Fig. 6.** EBSD characterization of the cross-section of CSP 7075 Al deposit after nanoindentation; (a) Euler angle map, (b) Euler angle map with LAGBs and (c) Image quality (IQ) map with the circles indicating regions with high local hardness (in GPa). (For interpretation of the references to color in this figure, the reader is referred to the web version of this article.)

machine (MTS, Systems Corporation, Eden Prairie, MN) under displacement control at constant cross-head speed of 1 mm/min. The applied load was measured continuously with a 25 kN load cell. The force required to shear off the coating and the coating/substrate attachment area then yielded the shear strength of the bond. This arrangement is shown in Fig. 1. As shown in this figure, three lugs were tested and the average shear strength was reported.

### 2.3.2. Micro- and nanohardness

Nanoindentation tests were conducted in load control with a maximum load of 10 mN while using a Berkovich indenter. An array of 121 indents with 10  $\mu\text{m}$  spacing in the  $x$  and  $y$  directions were made in order to obtain hardness measurements in different regions of the deposition, e.g. particle/particle interfaces and particle interiors. The Oliver and Pharr method [39] was used to determine hardness and modulus of the corresponding deposition. While the elastic modulus data was indeed obtained through this testing method, there was not significant variation in elastic modulus observed in the cold spray deposition. Thus, this data has been omitted from this report.

Vicker's microhardness measurements were also performed on the 7075 substrate and CSP layer using a Vicker's microhardness tester (HMV-2, Shimadzu, Tokyo, Japan) under an indenter load of 300 g. A microhardness traverse (collected from a substrate/coating cross-section) was conducted whereby measurements were obtained with a fixed separation of 0.3 mm, traveling from the substrate through the CSP/substrate interface and finally to the surface of the CSP layer. The position of the indentation relative to the CSP/substrate interface was measured using optical microscopy in conjunction with image analysis. For all the microhardness values reported in this paper, 10 measurements were collected and the standard deviations have been reported.

## 3. Results and discussion

### 3.1. Microstructural characterization

#### 3.1.1. As-received powder

Fig. 2 shows the morphology and surface grain structure of the feedstock powder particles characterized by SEM. From inspection of Fig. 2, most of the particles are spherical in shape with an

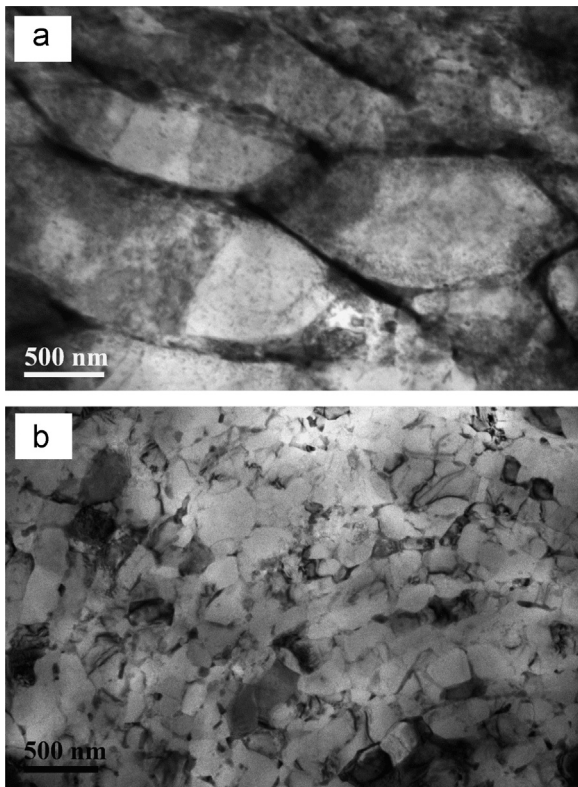


**Fig. 7.** TEM micrographs from (a) particle interiors showing the presence of larger grain size and higher dislocation density and (b) particle interfaces showing smaller sized dislocation free grains.

**Table 1**

Nanohardness obtained from the feedstock 7075 Al powder and CSP layer. Results include average  $\pm$  standard deviation.

Material	7075 powder		CSP 7075
	Particle interior	Particle-particle interfaces	
Hardness (GPa)	$1.35 \pm 0.24$	$1.53 \pm 0.30$	$2.01 \pm 0.09$

average particle size of  $18.6 \pm 8.2 \mu\text{m}$ . Micro-satellite particles (less than  $5 \mu\text{m}$  in size) are also present and observed either separated or attached to larger particles ( $\sim 10$  to  $25 \mu\text{m}$ ). Fig. 2(b) shows a typical powder particle with a diameter of  $\sim 20 \mu\text{m}$ . This image clearly shows that there is a  $\sim 1$  to  $3 \mu\text{m}$  external grain structure on the particle surface. Fig. 2(c) shows a back-scattered electron (BSE) micrograph of the as-received powder which has been polished in an epoxy resin. Based on the evident atomic number contrast (i.e. Z contrast) in this BSE image, it is speculated that there is a composition variation between grain boundaries (GBs) and grain interior. This observation and its effect on the final microstructure of different aluminum alloys have been well-addressed by the authors in previous studies [6,40–42].

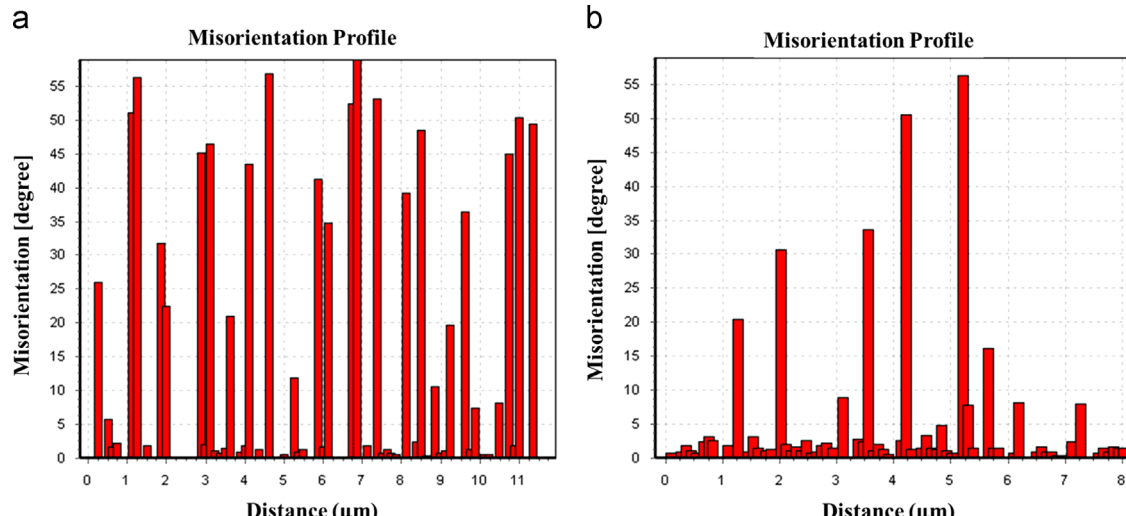
### 3.1.2. Cold sprayed deposition

Fig. 3 shows an optical micrograph from the etched cross-section (perpendicular to deposition) of the CSP 7075 coating. Macroscopically, the coating has a good deposition quality with very low porosity, few triple junction voids, and excellent bonding between powder particles. The coating deposition quality was uniform throughout the thickness of the coating. From inspection of Fig. 3, some regions of the 7075 deposited layer contain similar microstructure to that of the feedstock powder (see Fig. 2), whereas other areas are severely deformed. While powder particles undoubtedly undergo significant plastic deformation during HPCS, the interior of powder particles maintain a similar grain size and structure to the feedstock powder while particle-particle boundaries/interfaces are more heavily deformed. Thus, particle-particle interfaces experience significantly more plastic strain than particle interiors. The effect of this non-uniform strain distribution on the local mechanical properties has been evaluated by nanoindentation and is discussed in the next section.

### 3.2. Nanoindentation

Fig. 4(a) shows an optical micrograph of the square nanoindentation array (121 indentations) in the 7075 CSP layer. From inspection of Fig. 4(a), the testing area is free of voids or porosity. This is an important observation for these studies as the presence of porosity and voids can affect the size and depth of indentations during low load nanoindentation studies [43,44].

Fig. 4(b) presents a nanohardness contour map of the  $110 \mu\text{m} \times 110 \mu\text{m}$  test region. The map clearly shows a nonuniform



**Fig. 8.** Grain misorientation profiles for the (a) a particle-particle interface region, "A" in Fig. 6(b), and (b) a particle interior region, "B" in Fig. 6(b).

**Table 2**

Vickers microhardness measurements obtained from 7075 Al substrate and CSP layer subjected to various heat treatment conditions. Results include average  $\pm$  standard deviation.

Material	Substrate	CSP Layer As-Sprayed	CSP Layer Stabilized	CSP Layer Stabilized & aged
Hardness (Hv)	171 $\pm$ 5	115 $\pm$ 9	162 $\pm$ 3	170 $\pm$ 3

**Table 3**

Time and temperature conditions for the applied heat treatments [46].

Heat treatment	Temperature (°C)	Time (h)
Solutionizing	482	0.5
Stabilization	110	6
aging	162	24

hardness distribution in the deposited layer with some regions exhibiting higher hardness than others. Furthermore, Fig. 5 shows a histogram of the measured nanohardness in the cold spray deposition. Clearly, the hardness values are in the range of 1.20–2.10 GPa with the majority of hardness values in the range of 1.4–1.6 GPa. As can be seen in Fig. 4(a), the majority of indentations probe the particle interiors while the remainder are centered on the particle/particle interfaces. Therefore, it is expected that this nanohardness range (i.e. 1.4–1.6 GPa) is largely representative of the hardness of the particle interiors. This result may suggest a slightly higher nanohardness compared to the feedstock powder, which was measured to be  $1.35 \pm 0.24$ . This could be explained by the increase in dislocation density (DD) in the particle interiors compared with the as-received powder resulting from CSP [6]. These observations, especially the possible slight increase in nanohardness in the deposited material compared to the as-received powder, are consistent with previously published results on other cold sprayed materials [11,19,26–28,30].

EBSD mapping was also conducted for microstructural analysis and investigation of the observed variations in nanohardness. Fig. 6(a) depicts the Euler angle map of the test area. Clearly, the cold spray deposition grain structures (multicolored grains) and the residual indentations (black triangles) from nanoindentation testing can be observed. It is evident that there are two different grain size ranges in the microstructure. First, micron sized grains that are present in the particle interiors, and second, submicron sized grains that are mostly in the vicinity of particle–particle interfaces. Fig. 6(b) shows an EBSD map which reveals the high angle grain boundaries (HAGBs, black lines) and low angle grain boundaries (LAGBs, white lines) in the deposition microstructure. It is important to note that particle interiors are characterized by a higher density of LAGBs than particle–particle interfaces. This can also be seen in TEM micrographs in Fig. 7(a) and (b), which demonstrates the particle interiors and particle interfaces, respectively. Here particle interiors (Fig. 7(a)) are characterized by a larger grain size and higher dislocation density as compared to particle–particle interfaces (Fig. 7(b)), characterized by smaller grains with few dislocations. This observation provides evidence for the dynamic (and possibly static) recrystallization mechanisms that result in the formation of an UFG structure at particle–particle interfaces [6].

Fig. 6(c) shows an image quality (IQ) map for the area shown in Fig. 6(a,b). The circles indicate the locations for some of the highest obtained indentation values, and the numbers near the circles show the corresponding hardness values. As indicated in this figure, these high hardness values were measured in the vicinity of particle–particle interfaces. Moreover, using optical microscopy and EBSD analysis, the measured nanohardness for each indentation was correlated with its specific location in the microstructure (i.e. particle interior or particle–particle interface).

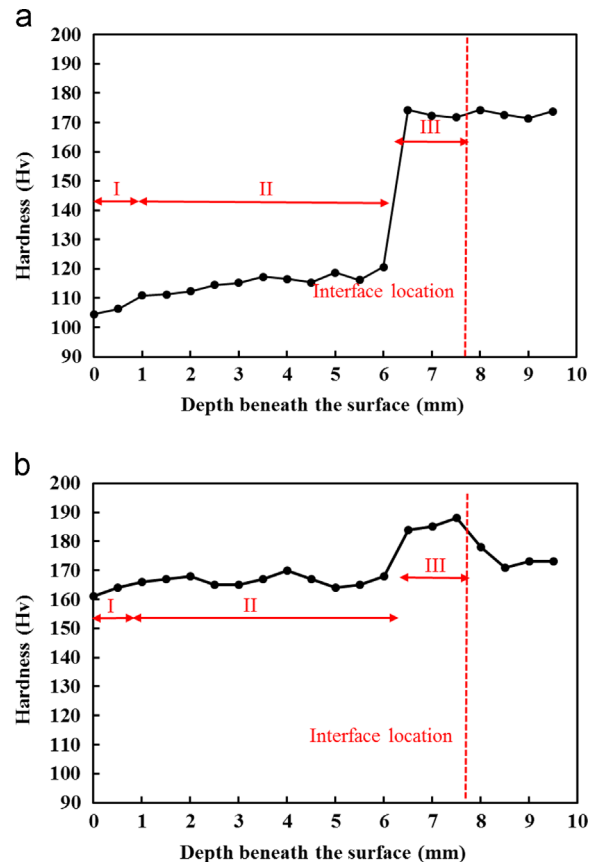


Fig. 9. Vickers microhardness distribution from the top of the CSP 7075 Al layer to the substrate, (a) before T-73 heat treatment, and (b) after T-73 heat treatment. The dashed red line represents the location of the deposit/substrate interface.

As such, Table 1 shows a summary of nanohardness values obtained from particle interiors and particle–particle interfaces and indicates a  $\sim 0.5$  GPa increase in nanohardness near particle–particle interfaces. Zou et al. [10] studied cold sprayed Ni and Cu and observed a roughly 1.5 GPa increase in hardness at particle–particle interfaces. The variation in hardness was attributed to smaller grain size (grain boundary strengthening) and higher dislocation densities (strain hardening strengthening) near particle–particle interfaces of the deposition. In the present study, however, although grain size indeed has a large influence on measured hardness at particle–particle interfaces, dislocation density likely plays a limited role. Fig. 8 shows the grain misorientation angles, obtained from EBSD, for a particle–particle interface region ("A" in Fig. 6(b)) and a particle interior region ("B" in Fig. 6(b)). From inspection of Fig. 8, the particle–particle interface region, Region "A", has a comparatively lower concentration of LAGBs (dislocation structures). In addition, while particle interiors contain a higher density of LAGBs, the measured hardness was similar to the as-received powder. Therefore, as seen in Table 1, it is believed that the higher hardness found at particle–particle interfaces is indeed largely associated with a smaller grain size (grain boundary strengthening), which developed during cold spray deposition.

### 3.3. Microhardness

**Table 2** shows the average microhardness values for the 7075 Al substrate and CSP 7075 Al layer. The CSP layer hardness ( $115 \pm 9$  Hv) was much lower than the substrate hardness ( $171 \pm 5$  Hv) which was in peak aged heat treatment condition. By comparison, the CSP layer hardness is slightly higher than the reported hardness for 7075 Al in solution treated, or W temper, condition (105 Hv [45]). To confirm that the metal feedstock powder and resulting deposition were in the solution treated condition, several sections of the CSP layer were excised and subjected to various heat treatments. The temperature and time conditions for the applied heat treatments (i.e. T-73 [46]) are presented in **Table 3**. As tabulated in **Table 2**, the hardness of the CSP layer reached that of the substrate after aging with the T73 heat treatment. As a result, it can be concluded that both the 7075 gas atomized feedstock powder and the resulting CSP layer were in the solution treated condition, since the deposit was responsive to the low temperature aging treatments. This slightly higher hardness in the CSP layer versus reported hardness for bulk 7075 Al in solution treated condition is most likely associated with strain hardening due to significant plastic deformation during cold spray deposition.

**Fig. 9** shows microhardness traverse measurements that were conducted by traveling from the substrate into the CSP layer with a fixed spacing of 0.3 mm. Measurements were conducted before (**Fig. 9(a)**) and after (**Fig. 9(b)**) heat treatment. The graphs were divided into three distinct regions (i.e. Regions I, II and III) for ease

of explanation. **Fig. 9(a)** shows the hardness traverse data for the CSP coating/substrate prior to heat treatment. Here, Region I shows that the lowest microhardness values were achieved near the coating surface of the CSP deposition. According to previously published results, the deposition quality near the surface often has a higher degree of internal porosity and lack of bonding, which may reduce the measured hardness (macro/microscopic) of the cold spray layer [6,25,47]. This observation is also indicative of a lower degree of plastic deformation (during deposition) in the final cold spray layers and may be associated with the absence of the so-called peening effect [47–50] in this region. The microhardness is slightly higher in Region II, even though the material is expected to have significant strain hardening in this area. Region III on the other hand, shows a significant increase in hardness in the area close to coating/substrate interface, approaching the substrate hardness. This increased hardness is possibly associated with two effects: firstly, a smaller grain size in this region, which could have resulted from an increased shot peening effect and larger plastic strains in this region, and second, precipitation hardening effect as has been already proven by authors that new precipitates are formed inter- and trans-granularly during cold spraying of 7075 deposition [6]. **Fig. 10** shows EBSD maps obtained from Regions I, II, and III and the corresponding grain size measurement. There is a steady reduction in grain size from the surface of the deposit to the interface.

**Fig. 9(b)** shows the microhardness traverse results for the CSP 7075 Al deposit after heat treatment. Clearly, the hardness in Regions I, II and III is significantly higher for the heat treated

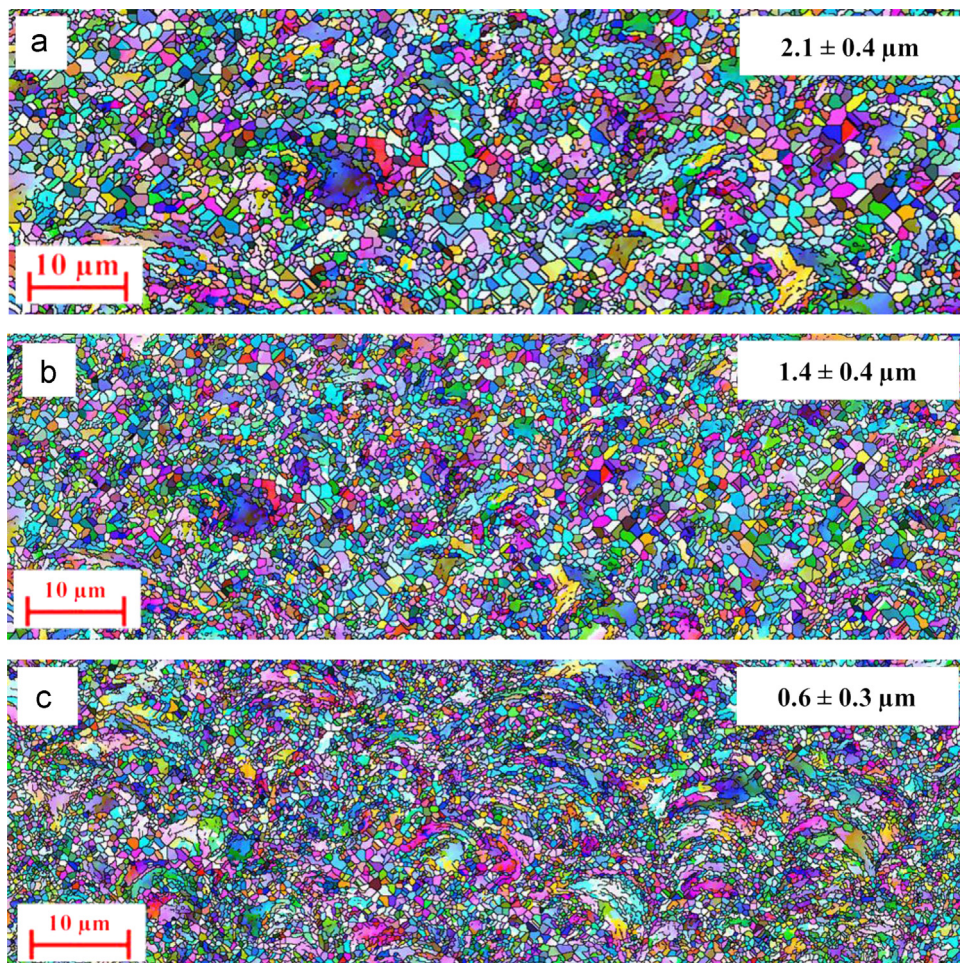


**Fig. 10.** EBSD maps from (a) top (region I), (b) middle portion (region II), and (c) bottom portion (region III) of CSP 7075 Al deposit. Upper right corner boxes show the average grain size in these regions.

**Table 4**

Summary of tensile and shear adhesion strength results for 7075 Al cold spray coatings on a 7075 Al substrate obtained by tensile pull-off and three lug shear testing. Results include average  $\pm$  standard deviation.

Tensile adhesion strength (MPa)	Shear adhesion strength (MPa)	Mode of failure
$83.8 \pm 1.75$	$92.4 \pm 1.9$	Cohesive

specimen and results in a more uniform hardness distribution across the CSP layer and substrate. As such, the hardness in the CSP layer more closely matches the level of the substrate material, and in some cases (Region III) exceeds the substrate hardness. As aforementioned, the area (Region III) near the deposit/substrate interface has substantially smaller grain size. As a result, the hardness value for this region has been affected by two factors, i.e. grain size and heat treatment.

#### 3.4. Bond strength

Bonding strength was also evaluated to investigate the effect of the microstructural variations on the quality of the deposition. Table 4 shows a summary of the tensile and shear adhesion strength results for 7075 Al cold spray coatings on a 7075 substrate obtained by ASTM C633 tensile pull-off and three lug shear testing, respectively. From inspection of Table 4, the tensile adhesion strength of the cold sprayed coating was  $83.8 \pm 1.75$  MPa. These bond strength values are higher than what is typically reported for other cold sprayed aluminum alloys, i.e. 40–70 MPa [51–54]. Table 4 also shows the shear adhesion strength, obtained by three lug shear testing, was  $92.4 \pm 1.9$  MPa. All of the tensile adhesion samples failed by cohesive failure in the surface layers of the deposit, and not at the coating/substrate interface. Typically, tensile pull-off values are higher than shear values, so presumably even higher adhesion strengths could have been achieved if the top layer had been removed. Regardless, these results indicate that the deposition reported here is of good quality and has excellent adhesion strength.

#### 4. Summary

This study investigates the relationship between the as-deposited cold spray microstructure and the resulting local and coating-scale mechanical properties of 7075 Al powder deposited onto wrought 7075 Al substrates via HPCS. Local mechanical property variation was probed using nanoindentation and correlated with microstructure characterization conducted via various microscopy techniques. Microstructure characterization revealed that particle interiors showed a larger grain size and higher dislocation density as compared to particle–particle interface regions (within the CSP deposition). Also, particle–particle interface regions had a roughly 0.5 GPa higher nanohardness as compared to particle interiors, which was attributed to local grain boundary strengthening caused by the formation of an UFG structure likely via dynamic recrystallization. Microhardness evaluation revealed the hardness of the solution treated CSP coating ( $115 \pm 9$  Hv) was much lower than the heat treated (T73) 7075 Al substrate ( $171 \pm 5$  Hv) and upon subsequent heat treatment the CSP coating hardness ( $170 \pm 5$  Hv) reached that of the substrate. Also, microhardness decreased with increasing distance from the substrate due to an increase in CSP layer grain size and associated reduction in the shot peening effect. Finally, the adhesion strength of the CSP layer was evaluated by tensile pull-off and three lug

shear testing methods with an average adhesion strength of 83.8 and 92.4 MPa, respectively.

#### Acknowledgments

The authors are grateful for the financial support of the U.S. Army Research Laboratory (ARL) under Contract no. W911NF-11-2-0014. Dr. S.P. Ahrenkiel is gratefully acknowledged for his assistance with electron microscopy. The authors also wish to thank Dr. B. Jasthi for his helpful discussions and assistance with the interpretation of results, and Mike Carter et al. for coordinating the deposition of the material for this analysis.

#### References

- [1] H. Koivuluoto, A. Milanti, G. Bolelli, L. Lusvarghi, P. Vuoristo, *J. Therm. Spray Technol.* 23 (2014) 98–103.
- [2] I. Ozdemir, K. Ogawa, K. Sato, *Surf. Coat. Technol.* 240 (2014) 373–379.
- [3] H. Koivuluoto, J. Nakki, P. Vuoristo, *J. Therm. Spray Technol.* 18 (2009) 75–82.
- [4] V.K. Champagne Jr., D. Helfritch, P. Leyman, S. Grendahl, B. Klotz, *J. Therm. Spray Technol.* 14 (2005) 330–334.
- [5] K. Ogawa, K. Ito, K. Ichimura, Y. Ichikawa, S. Ohno, N. Onda, *J. Therm. Spray Technol.* 17 (2008) 728–735.
- [6] M.R. Rokni, C.A. Widener, G.A. Crawford, *Surf. Coat. Technol.* 251 (2014) 254–263.
- [7] D. Goldbaum, R.R. Chromik, S. Yue, E. Irissou, J.G. Legoux, *J. Therm. Spray Technol.* 20 (2011) 486–496.
- [8] C. Borchers, F. Gartner, T. Stoltenhoff, H. Assadi, H. Kreye, *J. Appl. Phys.* 93 (2003) 10064.
- [9] C. Borchers, F. Gartner, T. Stoltenhoff, H. Kreye, *J. Appl. Phys.* 96 (2004) 4288.
- [10] Y. Zou, D. Goldbaum, J.A. Szpunar, S. Yue, *Scr. Mater.* 62 (2010) 395–398.
- [11] Q. Wang, N. Birbilis, H. Huang, M.X. Zhang, *Surf. Coat. Technol.* 232 (2013) 216–223.
- [12] H. Assadi, F. Gärtnner, T. Stoltenhoff, H. Kreye, *Acta Mater.* 51 (2003) 4379–4394.
- [13] G. Bae, Y. Xiong, S. Kumar, K. Kang, C. Lee, *Acta Mater.* 56 (2008) 4858.
- [14] M. Grujicic, J.R. Saylor, D.E. Beasley, W.S. DeRosset, D. Helfritch, *Appl. Surf. Sci.* 219 (2003) 211.
- [15] P.S. Phani, V. Vishnukanthan, G. Sundararajan, *Acta Mater.* 55 (2007) 4741.
- [16] W.Y. Li, C.J. Li, H.L. Liao, *J. Therm. Spray Technol.* 15 (2006) 206.
- [17] C. Borchers, F. Gartner, T. Stoltenhoff, H. Kreye, *Acta Mater.* 53 (2005) 2991.
- [18] T.H. Van Steenkiste, J.R. Smith, R.E. Teets, *Surf. Coat. Technol.* 154 (2002) 237–252.
- [19] D. Goldbaum, J.M. Shockley, R.R. Chromik, A. Rezaeian, S. Yue, J.G. Legoux, E. Irissou, *J. Therm. Spray Technol.* 21 (2012) 288–303.
- [20] Y. Xiong, G. Bae, X. Xiong, C. Lee, *J. Therm. Spray Technol.* 19 (2010) 575–585.
- [21] G. Rolland, P. Sallamand, V. Guipton, M. Jeandin, E. Boller, C. Bourda, *J. Therm. Spray Technol.* 21 (2012) 758–772.
- [22] J. Liu, H. Cui, X. Zhou, X. Wu, J. Zhang, *Met. Mater. Int.* 18 (2012) 121–128.
- [23] C.K.S. Moy, J. Cairney, G. Ranzi, M. Jahedi, S.P. Ringer, *Surf. Coat. Technol.* 204 (2010) 3739–3749.
- [24] J. Ajaja, D. Goldbaum, R.R. Chromik, *Acta Astronaut.* 69 (2011) 923–928.
- [25] L. Ajdelsztajn, B. Jodoin, J.M. Schoenung, *Surf. Coat. Technol.* 201 (2006) 1166–1172.
- [26] Y. Zou, W. Qin, E. Irissou, J.G. Legoux, S. Yue, J.A. Szpunar, *Scr. Mater.* 61 (2009) 899–902.
- [27] M.R. Rokni, C.A. Widener, A.T. Nardi, V.K. Champagne, *Appl. Surf. Sci.* 305 (2014) 797–804.
- [28] L. Ajdelsztajn, B. Jodoin, G.E. Kim, J.M. Schoenung, *Metal. Mater. Trans. A* 6 (2005) 657–666.
- [29] Y.Y. Zhang, X.K. Wu, H. Cui, J.S. Zhang, *Therm. Spray Technol.* 20 (2011) 1025–1032.
- [30] B. Jodoin, L. Ajdelsztajn, E. Sansoucy, A. Zúñiga, P. Richer, E.J. Lavernia, *Surf. Coat. Technol.* 201 (2006) 3422–3429.
- [31] P. Richer, B. Jodoin, L. Ajdelsztajn, E.J. Lavernia, *J. Therm. Spray Technol.* 15 (2006) 246–254.
- [32] Y. Chen, S.R. Bakshi, A. Agarwal, *Surf. Coat. Technol.* 204 (2010) 2709–2715.
- [33] S.R. Bakshi, V. Singh, K. Balani, D.G. McCartney, S. Seal, A. Agarwal, *Surf. Coat. Technol.* 202 (2008) 5162–5169.
- [34] D.J. Woo, B. Sneed, F. Peerry, F.C. Heer, L.N. Brewer, J.P. Hooper, S. Osswald, *Carbon* 63 (2013) 404–415.
- [35] M.R. Rokni, A. Zarei-Hanzaki, A.A. Roostaei, H.R. Abedi, *Mater. Des.* 32 (2011) 2339–2344.
- [36] M.R. Rokni, A. Zarei-Hanzaki, H.R. Abedi, *Mater. Sci. Eng. A* 532 (2012) 593–600.
- [37] J.P. Immarigeon, R.T. Holt, A.K. Koul, L. Zhao, W. Wallace, J.C. Beddoes, *Mater. Charact.* 35 (1995) 41–67.
- [38] MIL-J-24445A, Joint, Bimetallic Bonded, Aluminum to Steel, Department of Defense Military Specification, March 1, 1971.
- [39] W.C. Oliver, G.M. Pharr, *J. Mater. Res.* 7 (1992) 1564.

- [40] M.R. Rokni, C.A. Widener, V.R. Champagne, *Appl. Surf. Sci.* 290 (2014) 482–489.
- [41] M.R. Rokni, C.A. Widener, S.P. Ahrenkiel, B.K. Jasthi, V.R. Champagne, *Surf. Eng.* 30 (2014) 361–368.
- [42] M.R. Rokni, C.A. Widener, V.R. Champagne, *J. Therm. Spray Technol.* 23 (2014) 514–524.
- [43] H. Bu, M. Yandouzi, C. Lu, B. Jodoin, *Surf. Coat. Technol.* 205 (2011) 4665–4671.
- [44] D. Goldbaum, J. Ajaja, R.R. Chromik, W. Wong, S. Yue, E. Irisson, J.G. Legoux, *Mater. Sci. Eng. A* 530 (2011) 253–265.
- [45] A. Gerlich, G. Avramovic-Cingara, T.H. North, *Metall. Mater. Trans. A* 37 (2006) 2773–2786.
- [46] ASM Committee on Gas Carburizing, Carbonitriding, and Nitriding, Gas Nitriding, Heat Treatment: ASM Handbook, American Society of Metals, Materials Park, OH (1991) 191.
- [47] C.J. Li, W.Y. Li, *Surf. Coating Technol.* 167 (2003) 278–283.
- [48] O. Meydanoglu, J. Bertrand, E. Sabri Kayali, *Surf. Coat. Technol.* 235 (2013) 108–116.
- [49] T.H.V. Steenkiste, J.R. Smith, R.E. Teets, *Surf. Coat. Technol.* 154 (2002) 237–252.
- [50] M. Yandouzi, L. Ajdelsztajn, B. Jodoin, *Surf. Coat. Technol.* 202 (2008) 3866–3877.
- [51] E. Irisson, J.G. Legoux, B. Arsenault, C. Moreau, *J. Therm. Spray Technol.* 16 (2007) 661–668.
- [52] J. Wu, J. Yang, H. Fang, S. Yoon, C. Lee, *Appl. Surf. Sci.* 252 (2006) 7809–7814.
- [53] D. Zhang, P.H. Shipway, D.G. McCartney, *J. Therm. Spray Technol.* 14 (2005) 109–116.
- [54] S. Shin, Y. Xiong, Y. Ji, H.J. Kim, C. Lee, *Appl. Surf. Sci.* 254 (2008) 2269–2275.